THE VERIFICATION OF CHAOTIC CHARACTERISTICS OF RADAR ANGULAR GLINT

J. Zhang[*] and J. Miao

School of Electronic Engineering, Beihang University, Beijing, China

Abstract—In this paper, we present the chaotic verification for angular glint of complex radar target. Angular glint is a key factor in the generation loss probability in radar detections, and the intrinsic physical characteristic and suppression techniques of glint have been a hot topic in radar signal analysis. In this paper, the radar angular glint samples of a typical complex target are calculated by the Greco method based on Phase Gradient method. The simulated glint series fit the prerequisites of chaos for deterministic, nonlinear generation and no regularities in time domain, therefore the analysis the chaotic traits is required. We propose the design of chaotic verification flow, which is proved to be efficient and effective by the experiment of Lorenz Attractor signal model, and the details have been explained. The algorithm flow begins with the determination of optimum time lag and minimum embedding dimension, and is followed by the time-delay reconstruction in phase space. The results are presented with three qualitative verification results of attractor geometry, Poincare section and principal component analysis and two quantitative results of correlation dimension and largest Lyapunov exponent for the glint series. With comparison with results obtained by Lorenz attractor, the chaotic traits of angular glint data are verified. Therefore, the paper has proposed new possible reduction and prediction ideas to refrain angular glint in the digital processing unit of radar receiver in the future.

* Corresponding author: Jin Zhang (zhangjin850224@139.com).

1. INTRODUCTION

Since 1959, when the concept of glint was firstly proposed, the radar angular glint has attracted great attention among electro-magnetic diffraction and stealth researchers [1–3]. The angular glint is a key signal in the generation of target loss probability in radars, for strong glint can give rise to tracking loss and misjudgment. The concept of glint is interrelated with the concept of extended radar target. Any target that has dimensions compared with wavelength and is comprised of more than two scattering centers is regarded as an extended target, and any extended radar target can generate angular glint.

The angular glint and radar cross section (RCS) are two significant signals of target characteristics. Researchers have gained an insight into the relationship between RCS and angular glint. Some drew the conclusion that: (1) the two are negatively correlative; (2) they are neither correlative nor independent [4–6].

The primary cause of angular glint is the interactions among each reflection unit inside the extended target. When the radar is scanning, angular glint could cause the antenna to jitter, the result of which is the increase of target tracking loss probability. When the target travels nearer to the radar, this phenomenon is more evident. There have been a lot of published research results with the purpose of suppression of glint, and methods such as widening the angular range and space diversity have been applied in radar designs, but few have done researches of glint when regarded as a time series, which is the main topic of this paper.

In this paper, angular glint data of three typical trajectories of a typical extended target are calculated by the Greco method, which is accepted with sufficient accuracy compared with measurement results [7, 8]. The generation of angular glint is deduced from phase perturbation theories and has analytical expressions, therefore glint is not stochastic but deterministic. Moreover, there are no quasi-periodic or other regularities in glint data, both of which further propose the question of whether glint is chaotic. Therefore, an effective workflow of chaotic verification has been designed by the author. With the comparison of the results obtained by this workflow of Lorenz attractor, which is a typical model of chaos, the chaotic characteristics of angular glint are verified. The merit of these verifications is that if a time series is chaotic, it is predictable in a short future time range and the fluctuations can be decreased by related chaotic signal reduction methods. These algorithms can be integrated into the DSP unit of the radar receiver in the future to calibrate target position inaccuracies generated by angular glint effects.

2. GLINT CALCULATION BY GRECO

2.1. Greco Algorithm Explanation

As glint is not easily detected in radar operations, theoretical simulation methods are widely applied. Two types of glint generation theories of glint are accepted by the majority: the tilt of electromagnetic energy flow [8] and phase perturbation [2] theory. The first one is realized by the calculation of energy flow of the scattering field; the second is applied in the phase simulations of angular glint and is accurate compared with measurement results. It has been verified that in isotropic media and under geometrical optics approximations, the two techniques are identical [8]. The Greco method which is Graphical Electro-magnetic Computation was first developed by Spanish researchers for RCS real time calculation in 1993. It belongs to the phase perturbation method group. Several simulation results of glint of a typical targets are given [9].

We have developed a similar Greco software with a newly verified package for glint calculation, which is one novelty in electromagnetic scattering simulations [10, 11]. Compared with publicized measurement results, angular glint calculations by our package are accurate [11]. Each pixel on the computer screen is regarded as a scattering center and all the pixels of a target are calculated. All the equivalent scattering centers are classified in edge and surface types. The angular scintillation is computed for the target on a trajectory [10]. The target selected is the same as in reference [9].

The simulation setup and target is shown in Fig. 1. In the optical range, the scattering field of the target can be modeled as the vectorial sum of the echo fields of each scattering center. Let d_N be the distance between each scattering center, R and r_N are distances between the
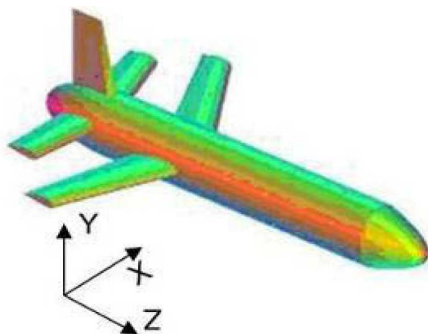

Figure 1. Target for GRECO simulation [9].

centers and the radar $(R \approx r_N)$, and $R \gg d_N$, $R \gg \lambda$, the total scattering field received can be derived as:

$$\mathbf{E^s} = \sum_{i=0}^{n} E_n^s \exp[-j(2kr_N - \delta_N)] \tag{1}$$

in which E_n^s and δ_N are the amplitude and phase of the scattering field. The relation between the incident and the scattering field is shown by (2), where subscript 1 or 2 denotes vertical or horizontal polarization of the incident or scattering field, and $[\mathbf{Q}]$ is the equivalent scattering matrix:

$$\begin{bmatrix} \mathbf{E_1^s} \\ \mathbf{E_2^s} \end{bmatrix} = \begin{bmatrix} Q_{11} & Q_{12} \\ Q_{21} & Q_{22} \end{bmatrix} \begin{bmatrix} \mathbf{E_1^i} \\ \mathbf{E_2^i} \end{bmatrix} \tag{2}$$

$$[\mathbf{Q}] = e^{i\varphi_{11}} \begin{bmatrix} \sqrt{\sigma_{11}} & \sqrt{\sigma_{12}}e^{i(\varphi_{12}-\varphi_{11})} \\ \sqrt{\sigma_{21}}e^{i(\varphi_{21}-\varphi_{11})} & \sqrt{\sigma_{22}}e^{i(\varphi_{22}-\varphi_{11})} \end{bmatrix} \tag{3}$$

where $\sqrt{\sigma_{1,2}}$ and φ_{11} are the amplitude and phase of the scattering field for different polarizations. It can be seen from (2) that when the incident wave is spherical, the wave front of the scattering field is astigmatic, whose curvature is shown in $[\mathbf{Q}]$. The curvature radius of the scattering fields for two polarizations is given by:

$$\frac{1}{\rho_{1,2}} = \frac{1}{2} \left[Q_{11} + Q_{22} \pm \sqrt{(Q_{11} - Q_{22})^2 + 4Q_{22}^2} \right] \tag{4}$$

With the target DXF model (perfect conductor) and Greco method, the back-scattering fields are simulated by (5), Where the scattering field of the nth surface and the nth edge are represented by $\mathbf{E_n^s}$ and $\mathbf{E_n^d}$, and the total scattering field is their vectorial sum by (6):

$$\begin{cases} \mathbf{E_\perp^s} = \sum_{n=1}^{N} \left(\mathbf{e_{n\perp}^i} \cdot \mathbf{E_n^s} + \mathbf{e_{n\perp}^i} \cdot \mathbf{E_n^d} \right) \\ \mathbf{E_\parallel^s} = \sum_{n=1}^{N} \left(\mathbf{e_{n\parallel}^i} \cdot \mathbf{E_n^s} + \mathbf{e_{n\parallel}^i} \cdot \mathbf{E_n^d} \right) \end{cases} \tag{5}$$

$$\mathbf{E^s} = \sum_{n=1}^{N} \left(\mathbf{e_n^i} \cdot \mathbf{E_n^s} + \mathbf{e_n^i} \cdot \mathbf{E_n^d} \right) \tag{6}$$

Above all, under the irradiation of uniform plane or spherical wave, the beam front of the target is astigmatic with the phase front by (7), in which $[b]^T = [R\boldsymbol{\theta} + R\boldsymbol{\varphi}], [\mathbf{r}, \boldsymbol{\theta}, \boldsymbol{\varphi}]$ is the unit vector in spherical coordinate, $\mathbf{Q}(R)$ is the curvature matrix of the scattering wave. The angular glint of a complicated target can be deducted using the phase gradient method by (8) [11]. It can be observed from formula (7) and (8) that angular glint is related not only to R, but also the astigmatic beam front $[b]$, This relationship is a quadric surface expression. The edge and surface scattering centers are all included in these simulations.
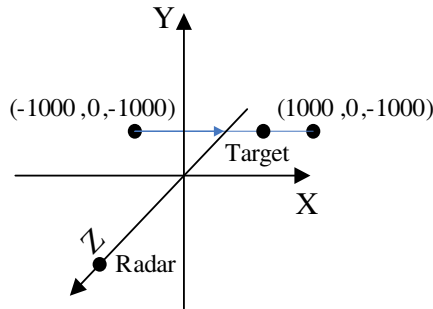
Figure 2. Target trajectory for straight line movement.

These expressions show that the azimuth and elevation plane angular glint series are all generated by nonlinear calculations of phase perturbations, which are prerequisite for further chaotic discussions.

$$\phi = \frac{2\pi}{\lambda}\left\{R + \frac{1}{2}[b]^T Q(\mathbf{r})[b]\right\} \tag{7}$$

$$\begin{cases} e_\theta = \dfrac{r(\nabla\phi)\theta}{(\nabla\phi)R} \\[2mm] e_\varphi = \dfrac{r(\nabla\phi)\varphi}{(\nabla\phi)R} \end{cases} \tag{8}$$

2.2. Glint Calculations Using Greco

In this paper, three types of target trajectory are selected, they are the straight line, spiral and rotary trajectories, respectively. These trajectories are chosen to cover most frequent target movement styles [12, 13]. The target dimension (compared with wavelength) and radar detection distance meet the requirement of far field.

The first simulation of straight line motion (glint 1) is calculated, which is the simplest type of trajectory for a target. The target movement is shown in Fig. 2.

The second simulation setup is the rotary motion (glint 2), which yields much larger fluctuations in glint values than glint 1. The target moves in the orthogonal plane to the vector around the origin. The target movement is shown in Fig. 3. The third simulation is done by the spiral motion of the target, in which the target moves in a circle around a fixed point (glint 3). The target movement is shown in Fig. 4.

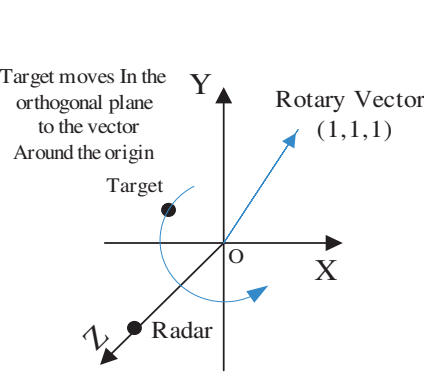The simulation parameters are summarized in Table 1.
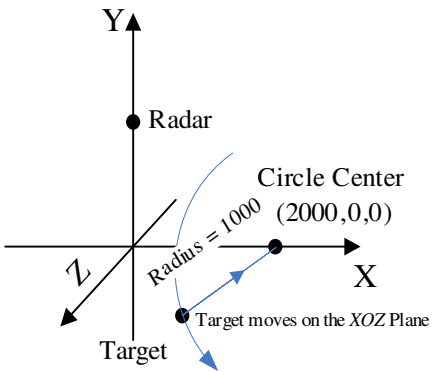
Figure 3. Target trajectory for rotary movement.

Figure 4. Target trajectory for spiral movement.

Table 1. Glint calculation parameters using GRECO.

Motion	Straight Line	Rotary	Spiral
Frequency	10 GHz	20 GHz	10 GHz
Polarization	VV	VV	VV
Incident Electric Field Intensity	1 V/m	1 V/m	1 V/m
radar position	$(0, 0, 1000)$	$(0, 0, 1000)$	$(0, 2000, 0)$
Model In Simulation	surface & edge	surface & edge	surface & edge
Calculation Plane	Azimuth	Azimuth	Azimuth
Glint Unit	m	m	m
Calculation Pts	3600	18000	3600

3. THE DESIGN OF THE CHAOTIC VERIFICATION FLOW AND USABILITY CHECK BY THE LORENZ MODEL

Nonlinear science and chaotic theories have been hot topics in the researches of signal processing, from which many previously insolvable problems have found new solutions. In economical, geographical and meteorological signal analysis, nonlinear and chaotic algorithms have been widely applied and accepted. Previous chaos verifications are done by independent methods such as

attractor geometry formation, primary component analysis and largest Lyapunov exponent calculations, but few papers have discussed an intact and efficacious verification workflow which combines most of the independent methods. Based on chaotic principles, this workflow is designed and the performance is verified by Lorenz model (publicly known chaos model), and the verification criteria are summarized. This section focuses on the algorithm development and performance check. Then, the flow is applied to verify that the three angular glint series are chaotic.

3.1. Chaotic Verification Workflow Design and Descriptions

The work flow is shown in Fig. 5.

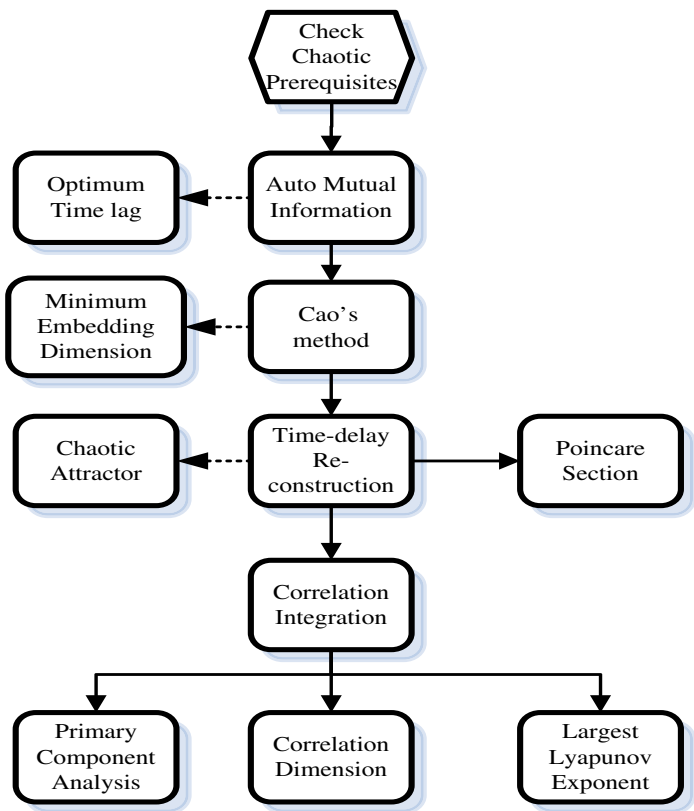Verification criteria are divided to qualitative and quantitative

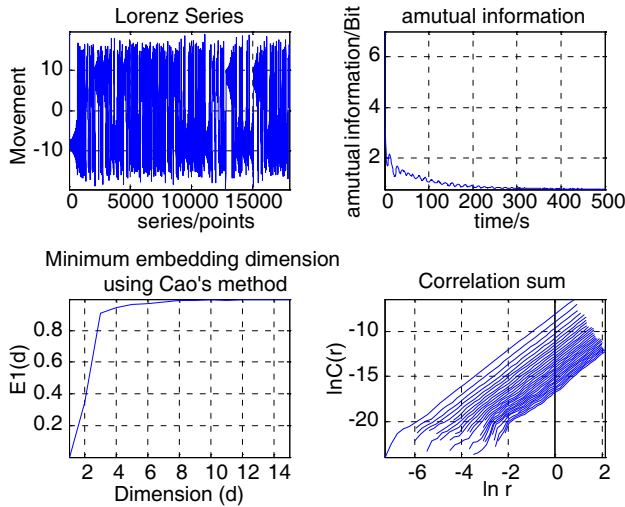**Figure 5.** Chaotic verification flow designed by the author.

Figure 6. Workflow step illustration of lorenz model.

ones. The three typical qualitative chaotic criteria include chaotic attractor geometry, Poincare section, and PCA (Principal Component Analysis), and they are depicted by figures. Two most frequently used quantitative chaotic criteria are: correlative dimension and largest Lyapunov exponent, and they are shown by values. These chaotic criteria are all contained in the work flow, which has been verified to be effective in distinguishing chaotic or not by Lorenz Attractor model. To help understanding, each important step is accompanied by a figure.

The work flow is applied from top down. The input time series could be Lorenz Model, or angular glint series. The verification steps are illustrated below:

1. Check the chaos prerequisite: whether the data is generated by deterministic and nonlinear relations. Moreover, no regularities could be found in time and frequency domains.

2. Obtaining the optimum time lag. The first step is to determine the optimum time lag for phase space reconstruction by the auto mutual information function. A large number of time lags are used to calculate average auto mutual information values, and the corresponding reconstruction of the original time series is given. The time delay of the first minimum value of the reconstructed time series is selected as the estimation of optimum time lag [14, 15]. This procedure can be observed from the upper-left of Fig. 6. The setup of Lorenz model will be explained in the next section.

3. Minimum embedding dimension determination by Cao

method [16]. Firstly, using the optimum time lag τ and $d + 1$ (embedding dimension to be determined) and the fake nearest neighbor algorithm, the norm division parameter $E1(d)$ is obtained, and after weighting sum and normalization operations, the figure of $E1(d)$ is drawn. Secondly, the minimum embedding dimension (min-ed) is set as the first obvious inflection point of $E1(d)$. Thirdly, the chaotic attractor is reconstructed using τ and min-ed, and its movement characteristics are shown in the figure. Generally speaking, min-ed the should be 2 or 3 to successfully reconstruct the dynamic traits of attractors. Once this minimum embedding dimension is obtained, then phase space reconstruction can be done. This procedure is shown in the lower-left of Fig. 6, and an apparent inflection point appears in embedding dimension of 3.

The first chaotic qualitative criterion obtained by this procedure is summarized as: If the attractor moves with large dimensions and folds often in the limited space, and the movement is neither intersected nor in a periodic version, the time series is regarded to possess chaotic traits. Often, the "cloud" or "star" shape attractors are more convincing than other shapes in diagnosing chaos by attractor geometry [17, 18].

4. Phase space reconstruction and the generation of Poincare section of 2 or 3 dimensions [18]. Firstly, the phase space reconstruction is done based on the minimum embedding dimension. Secondly, one typical cross section plane should be selected to facilitate the observation of phase space movement. This selection is the Poincare section, and should be made with no overlapping with the trajectory planes or the planes that are orthogonal to them. The movement of the phase-space reconstruction is then intersected with the Poincare plane, and hundreds of cross section points form the Poincare points sequence $(B_0, B_1, \ldots, B_n)$. Mappings are needed to decrease the movement dimension of these points, and this mapping is called the Poincare mapping $\mathbf{T}$:

$$B_{n+1} = \mathbf{T}B_n$$

After mapping, the Poincare point figures can be shown. The second chaotic qualitative criterion is summarized as [19]: (1) If there are only a small number of stationary points in the Poincare point figure, the time series is periodic; (2) If the points form a closed curve, the time series is quasi-periodic; (3) If the points form structures that possess fractal structures or the geometry is in structures other than (1) and (2), the time series is chaotic. Also, the boundaries of dense and sparse distributions of intersection points should be clear. For practical observation convenience, two dimension Poincare Section figure is sufficient to obtain the dynamic traits of the time series [19].

5. The calculation of correlation dimension by the correlation integration G-P algorithm [18, 19]. Firstly, using the minimum embedding dimension obtained in step 3 to reconstruct phase space and calculate the correlation integration curve; Secondly, increase the embedding dimension one by one to observe the correlative dimension curves. The selection of the correlation dimension is to eliminate the curves that have zero or infinite slopes and find the curve that is nearest to a straight line. The slope of this curve is set as the correlation dimension D. Finally, inspect the convergence of these correlation dimension curves. If the curves that have larger embedding dimensions approximately converge to a fixed point, then the slope of this curve (D) is the optimum embedding dimension opt-ed. This procedure is shown in the lower-right of Fig. 6, from which it is seen that the distances between each correlation sum curve is closer (the upper-left is the starting curve), and the curve that is most similar to a straight line appears in the mid-range of the curve group. The correlation dimension result is shown in Table 2.

The first chaotic quantitative criterion can be expressed as [17–19]: (1) If D is an integer, then the time series is quasi-periodic or stochastic; (2) If D is a fraction, then the time series is chaotic.

6. The phase-space reconstruction using opt-ed and the Principal Component Analysis [14, 19, 20]. Firstly, use the optimum time lag and embedding dimension to reconstruct the phase-space, and calculate the trajectory matrix; then deduce the covariance matrix of this trajectory matrix, and obtain the eigen-values and eigenvectors; Secondly, rearrange the eigen-values from the minimum to the maximum, then the eigen-values and their corresponding eigenvectors are regarded as the principal components of the time series. Finally, sum up all the eigen-values for each embedding dimension (from 1 to opt-ed) to obtain a figure with eigen-value sum γ as Y coordinate and embedding dimension as X coordinate.

The third chaotic qualitative criterion (Principal Component Analysis, PCA) is summarized as [19, 20]: (1) If the PCA values are depicted as a straight line which has nearly zero slope, the time series is stochastic or periodic; (2) If the PCA values are decreasing with a negative slope, and with steep decline in low embedding dimensions, then the time series is chaotic.

7. The calculation of Largest Lyapunov Exponent by the Wolf method [21]. The fundamentals of the Wolf method derive from the nearest neighbor algorithm. Firstly, define an initial threshold distance value and set a starting point from the time series after the phase-space reconstruction, then determine the nearest point. Secondly, track the time domain development of these two points until the distance

between the two points are larger than a threshold value. Thirdly, keep the information of the two points then repeat the previous step to find the third nearest point. The angular distance (distance between the first two points measured as an angle from the third point) should be minimum in choosing this point. Fourthly, repeat the previous steps for all the points in the phase-space reconstructed time series until the end of series, and use the weighting average of the logarithm distance quotients of these distances to deduce the curve of Lyapunov exponent.

The largest value of this curve is the second quantitative chaotic criterion: (1) this value is larger than zero; (2) the order of magnitude of this value for a test time series is the same as the order quantity of a typical chaotic time series model, then the time series in test is chaotic rather than periodic or stochastic.

3.2. The Setup of the Lorenz Model and Workflow Usability Check

The typical Lorenz Model is established for verification of the effectiveness of this work flow. Lorenz model is one of the accepted chaotic model whose iterative differential equations are shown in (9). The time step is chosen as 0.025, and the constants σ, r, b are set as 0.1, -0.1 and 0.02, data length is 18000 and the x axis series is simulated. In this simulation, the trace of time series is in normalized length, therefore no dimension is shown in the upper-left of Fig. 7.

$$\begin{cases} \dfrac{dx}{dt} = -\sigma(y - x) \\ \dfrac{dy}{dt} = -xz + rx - y \\ \dfrac{dz}{dt} = xy - bz \end{cases} \tag{9}$$

The prerequisite check for Lorenz model is not required, for it is a standard chaotic system. The qualitative verification for Lorenz model is shown in Fig. 7. From the upper-right figure, the Lorenz model attractors extend and fold in the limited space with no intersections or periodic movements, and the structure is cloud-like. From the lower-left figure, the Poincare Sections possesses fractal structures, and is not formed by stationary points or closed curves, and the boundaries are clear. From the lower-right figure of PCA, the PCAs of Lorenz model are decreasing with a negative slope, and declines are steeper in lower dimensions, especially from 1 to 3. The quantitative results of Lorenz model is shown in Table 2. It is observed that the correlation dimension is not integer, and the largest Lyapunov exponent is larger
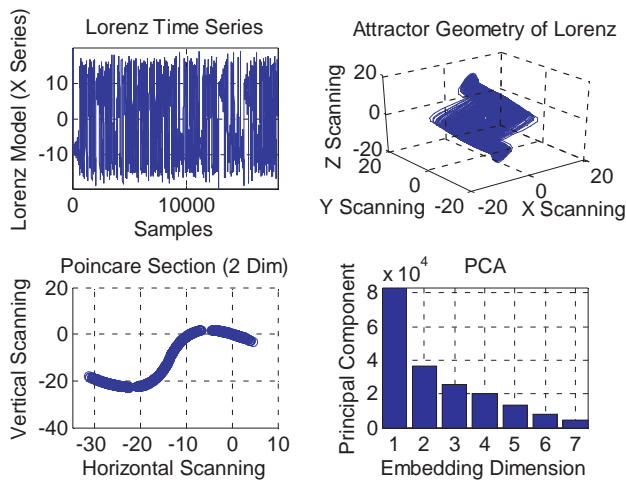
Figure 7. Workflow usability check by Lorenz model (qualitative results).

Table 2. Quantitative chaotic verification results.

Time Series	Correlation Dimension	Largest Lyapunov Exponent
Lorenz Model	1.9841	0.0768

than zero, both of which prove that this verification workflow is able to detect chaos effectively.

4. THE CHAOTIC VERIFICATION RESULTS FOR ANGULAR GLINT AND ANALYSIS

4.1. Qualitative Chaotic Verification Results and Analysis

Based on the chaotic verification flow, the qualitative verification results of Attractor Geometry, Poincare Section (2 Dim), and PCA are shown below from Fig. 8 to Fig. 10.

Firstly, the prerequisite should be checked. In our case of glint data, they are all generated by nonlinear mathematic expressions, and no clear regularities (quasi-periodic or others) can be found.

From the upper-right four figures of attractor geometries, the Lorenz model and the other three glint attractors all extend and fold in the limited space with no intersections or periodic movements. The
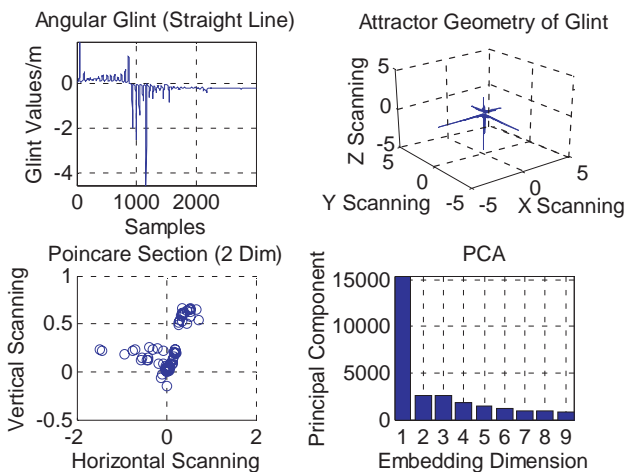
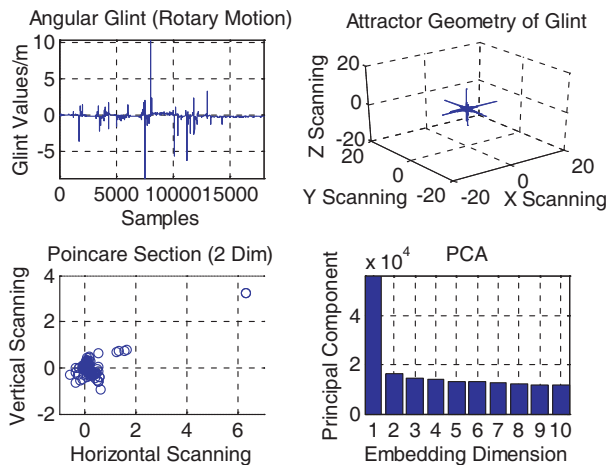**Figure 8.** Qualitative chaotic verification for straight line glint.

Figure 9. Qualitative chaotic verification for rotary motion glint.

geometry structures of the three angular glints are clear and are all star-like.

From the lower-left three figures of Poincare Sections, the three glint Poincare sections all possess fractal structures, and these sections are neither formed by stationary points nor closed curves. The boundaries of the dense and sparse distributions of Poincare Sections of glint series are clear.
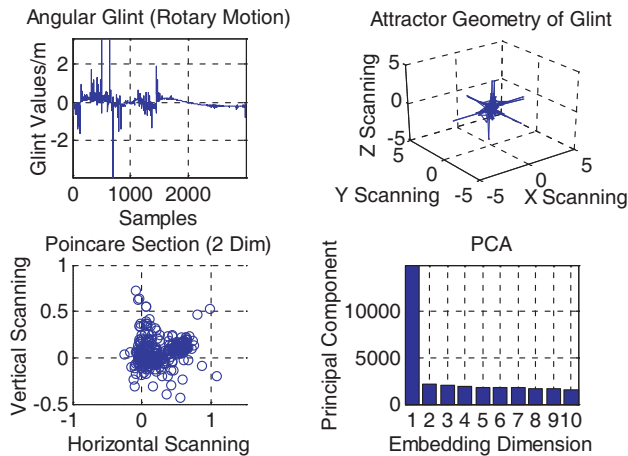
Figure 10. Qualitative chaotic verification for spiral motion glint.

Table 3. Quantitative chaotic verification results.

Time Series	Correlation Dimension	Largest Lyapunov Exponent
Angular Glint 1 (Straight Line)	1.7709	0.0171
Angular Glint 2 (Rotary Motion)	2.0733	0.0723
Angular Glint 3 (Spiral Motion)	1.8842	0.0159

From the lower-right three figures of Principal Component Analysis, the three glint series PCA all decrease in negative slopes, and the declines are steeper in lower embedding dimensions, such as from 1 to 5.

Therefore, on the basis of the above qualitative chaotic verification results and with comparison of results obtained from Lorenz model, the three angular glint series all possess clear chaotic traits.

4.2. Quantitative Chaotic Verification Results and Analysis

Based on the chaotic verification flow, the quantitative verification results of largest Lyapunov exponent and correlation dimension are shown in Table 3.

It can be observed that the correlation dimensions of the time series are all fractal; the largest Lyapunov exponents are all larger than zero. More importantly, the correlation dimensions and the largest

Lyapunov exponents of angular glint series are all in the same order of magnitude as Lorenz model. Therefore, on the basis of the two quantitative chaotic verification criteria, the three angular glint series are all chaotic.

5. CONCLUSION

The chaotic verification flow designed by the author is presented in this paper and the verification of chaotic traits for angular glint series of a typical target is verified. Firstly, as angular glint is not easily captured by radars, one typical extended radar target is selected, and the glint series applied in this paper are calculated by a newly developed package, which is the first novelty of this paper. Secondly, when treated as time series, glint is deterministic (from its generation calculations) but no clear regularities are found, which fits the prerequisite for chaos, therefore the question to verify chaos is raised. A clear and effective chaotic verification flow which is illustrated in detail is designed by the author (the second novelty of this paper), and its effectiveness is verified by the Lorenz Attractor model, which is a typical chaotic model. Then, the three glint series are verified by the same flow with chaotic prerequisites checked. Compared with the results of Lorenz Attractor and the chaotic verification criteria, the chaotic characteristics of angular glint are demonstrated with qualitative and quantitative results, which form the third novelty of this paper.

Once the chaotic characteristics are proved, the research of angular glint can make one step further. Chaos and related topics in nonlinear science have been widely applied in the data analysis of economics, meteorology and geo-science. Chaotic signals can be effectively suppressed by related algorithms and predicted in a small future time period, both traits are very significant in angular glint analysis. Therefore, there is no reason to refuse the application of chaotic theories in radar angular glint analysis, based on the research results in this paper.

REFERENCES

1. Howard, D. D, "Radar target glint in tracking and guidance system based on echo signal phase distortion," *Proc. of NEC*, 840–849, May 1959.
2. Lindsay, J. E, "Angular glint and the moving, rotating, complex radar target," *IEEE Trans. on Aerospace and Electronics Systems*, Vol. 4, 164–173, Mar. 1968.

3. Dunn, J. H. and D. D. Howard, "Radar target amplitude angle and Doppler scintillation from analysis of the echo signal propagating in space," *IEEE Trans. on Microwave Theory and Techniques*, Vol. 16, No. 9, 715–728, Sep. 1968.

4. Sinm, R. J. and E. R. Graf, "The reduction of radar glint by diversity techniques," *IEEE Trans. on Antenna and Propagation*, Vol. 19, No. 4, 462–468, 1971.

5. Ostrovityanov, R. V. and F. A. Basalov, *Statistical Theory of Extended Radar Targets*, Ch. 1–Ch. 3, Translated from Russian (Barton. W. F, Barton. D. K), Artech House, MA, 1985.

6. Stadhu, G. S. and A. V. Saylor, "A real-time statistical radar target model," *IEEE Trans. on Aerospace and Electronics Systems*, Vol. 21, No. 4, 490–507, 1985.

7. Yin, H. C., S. Deng, Y. Ruan, et al., "On the derivation of angular glint from backscattering measurements of each relative phase," *Acta Electronica Sinica*, Vol. 9, 36–40, 1996 (in Chinese).

8. Yin, H. C. and P. K. Huang, "Unification and comparison between two concepts of radar target angular glint," *IEEE Trans. on Aerospace and Electronics Systems*, Vol. 31, No. 2, 778–783, 1995.

9. Juan, M. R., M. Ferrando, and L. Jofre, "GRECO: Graphical electromagnetics computing for RCS prediction in real time," *IEEE Antennas and Propagation Magazine*, Vol. 35, No. 2, Apr. 1993.

10. Qin, D., "All-band electromagnetic scattering computation for complex targets: Method studies and application software," Ph.D. Dissertation, Department of Electrical Engineering, Beijing University of Aerosnautics and Astronatics, Beijing, P. R. China, 2004 (in Chinese).

11. Ning, H., N. Fang, and B. Wang, "Visual computing method of radar glint for complex target," *Chinese Journal of Electronics*, Vol. 15, No. 2, 356–358, 2006 (in Chinese).

12. Kazimierski, W., "Statistical analysis of simulated radar target's movement for the needs of multiple model tracking filter," *International Journal on Marine Navigation and Safety of Sea Transportation*, Vol. 5, No. 3, Sep. 2011.

13. Li, X. R. and V. P. Jilkov, "A survey of maneuvering target tracking — Part V: Multiple-model method," *IEEE Transactions on Aerospace and Electronic Systems*, Vol. 41, 2005.

14. Wolf, A. and T. Bessior, "Diagnosing chaos in the space circle," *Physica D: Nonlinear Phenomena*, Vol. 50, No. 2, 239–258, 1991.

15. Meiss, J. D., "Asked questions about nonlinear science,"

http://amath.colorado.edu/pub/dynamics/papers/sci.nonlinear-FAQ.pdf.

16. Cao, L., "Practical method for determining the minimum embedding dimension of a scalar time series," *Physica D: Nonlinear Phenomena*, Vol. 110, Nos. 1–2, 43–50, 1997.

17. Campbell, D. K., "Nonlinear science from paradigms and practicalities," *Los Alamos Science*, Vol. 15, 218–262, 1987.

18. Grassberger, P. and I. Procaccia, "Characterization of stranger attractors," *Phys. Rec. Lett.*, Vol. 50, No. 5, 346–349, 1983.

19. Lv, J. and J. Lu, *Chaotic Time Seires: Analysis and Applications*, 52–241, Wuhan University Press, Wuhan, 2002 (in Chinese).

20. Merkwirth, C., U. Parlitz, et al., *TSTOOL User Manual*, http://www.dpi.physik.uni-goettingen.de/tstool/manual.pdf.

21. Wolf, A., J. B. Swift, L. Swinney, et al., "Determining Lyapunov exponents from a time series," *Physica D: Nonlinear Phenomena*, Vol. 16, No. 3, 285–317, 1985.